PHYSICAL REVIEW B VOLUME 4, NUMBER 9 1 NOVEMBER 1971

Optical Spectrum of Cr^{3+} Pairs in $LaAlO_3$

J. P. van der Ziel
Bell Telephone Laboratories, Murray Hill, New Jersey 07974

(Received 15 March 1971)

The optical spectrum and exchange splittings of the nearest-neighbor Cr^{3+} pairs in $LaAlO_3$ have been studied. The absorption and emission spectra of the ${}^4A_2{}^4A_2 \longleftrightarrow {}^2E{}^4A_2$ pair transitions from 7200 to 7600 Å yield the ground-state exchange $-J^{ab}(\vec{S}^a\cdot\vec{S}^b)+j(\vec{S}^a\cdot\vec{S}^b)^2$ with $J^{ab}=-66.6$ cm^{-1} and $j=-0.76\,\text{cm}^{-1}$. The emission lines were studied as a function of uniaxial stress applied along the trigonal axis. The stress dependences of the pair lines are not very different from the single-ion shifts. The energy levels of the ${}^2E{}^4A_2$ and ${}^2E{}^2E$ pair states have also been determined. The latter corresponds to exciting both ions to the ${}^2E$ state, and the absorption is in the ultraviolet at about twice the ${}^2E$ single-ion energy. The excited-state splittings are compared with the values calculated from $\mathcal{H}_{ex}=-\sum J_{ij}\vec{s}_i\cdot\vec{s}_j$, where the sums are over the electronic spins $\vec{s}_i$ and $\vec{s}_j$ of the Cr^{3+} t_{2g} orbitals and the J_{ij} are empirical parameters. For the ${}^2E{}^4A_2$ levels we find that $J_{11}=-531.1\,\text{cm}^{-1}$ and $\frac{1}{2}(J_{12}+J_{21})=55.4\,\text{cm}^{-1}$ are the dominant exchange parameters. The signs and relative magnitudes agree with Anderson's theory. The pair lines have electric dipole polarization, and the strongest transitions obey the selection rule $\Delta S=0$, $\Delta M_s=0$. The polarization agrees with the calculated selection rules of the exchange-induced spin-dependent dipole moment $P=\sum P_{ij}\vec{s}_i\cdot\vec{s}_j$.

I. INTRODUCTION

The optical spectrum resulting from exchange-coupled Cr^{3+} pairs has been of considerable interest in recent years. Both for historical reasons and because of the ready availability of ruby as a laser host, the pair spectrum associated with the Cr^{3+} ${}^2E$-to-${}^4A_2$ transition in dark ruby has by far been investigated in the greatest detail.[1] The great complexity of the spectrum results from the structural fact that the exchange interaction between the ions of the pairs is appreciable up to the fourth neighbors. In addition the strong coupling with many inequivalent possible neighbors is responsible for the rapid migration of the excitation between single ions and pairs in the excited state of ruby, and for the Davydov splittings of the ${}^2E$ state in the concentrated material Cr_2O_3. The spectral complexity has reduced the ruby pair investigations to a cataloging of the lines according to the type of neighbor pair responsible for the emission and the values of the total spin $\vec{S}$ and z component of spin, M_s, of the levels.

The exchange interaction between two Cr^{3+} ions is given by

$$\mathcal{H}_{ex}=-\sum_{ij} J_{ij}\,\vec{s}_i^{\,a}\cdot\vec{s}_j^{\,b}\,, \tag{1}$$

where $\vec{s}_i^{\,a}$ is the spin of orbital i on atom a, and J_{ij} is a measure of the exchange. The sums are over the three t_{2g} electrons which make up the ${}^4A_2$ and ${}^2E$ states. The ground-state single-ion levels are coupled to yield states with total spin $S=0$, 1, 2, and 3. The interaction acting on the pair can be expressed in the form[2,3]

$$\mathcal{H}_{ex}=-J^{ab}\vec{S}^a\cdot\vec{S}^b+j(\vec{S}^a\cdot\vec{S}^b)^2+V^{ab}\,, \tag{2}$$

where

$$J^{ab}=\tfrac{1}{9}\sum_{ij}J_{ij} \tag{3}$$

and $\vec{S}^a$, $\vec{S}^b$ are the total spins of the two ions. The second term is a higher-order correction to the exchange, and V^{ab} expresses the remaining interactions which are small for the ground state.

The singly excited pair with one of the ions in the ${}^2E$ state and the other in the ${}^4A_2$ consists of eight states, four having $S=1$ and four with $S=2$. Since the first term in Eq. (2) obtains from Eq. (1) only for half-filled shells having the maximum multiplicity, it does not apply to the exchange splitting of the ${}^2E$ states.[4] Thus it is not surprising that the initial attempt by Clogston using the first term of Eq. (2) and the combined effect of crystal-field and spin-orbit splitting failed to explain the splitting of the singly excited pairs in ruby.[5,6]

The necessity of using Eq. (1) for the excited-state exchange has recently been realized.[1,7,8] However, the above-mentioned complexity of the ruby spectrum which is further complicated by the low symmetry of the pair sites has prevented the comparison of these theories with experiment. In order to connect with theory it is clearly of interest to examine the Cr^{3+} pair spectrum in a structurally simpler host such as $LaAlO_3$ which yields a predominantly large first-nearest-neighbor exchange as well as a relatively high symmetry pair.

The results of our investigation are presented in this paper. Section II reviews the structure, and the near-infrared emission and absorption is discussed in Sec. III. The emission spectrum was previously investigated by Blazey and Burns,[9] who found $J^{ab}=-39.8$ cm^{-1} and later by Tkachuk and

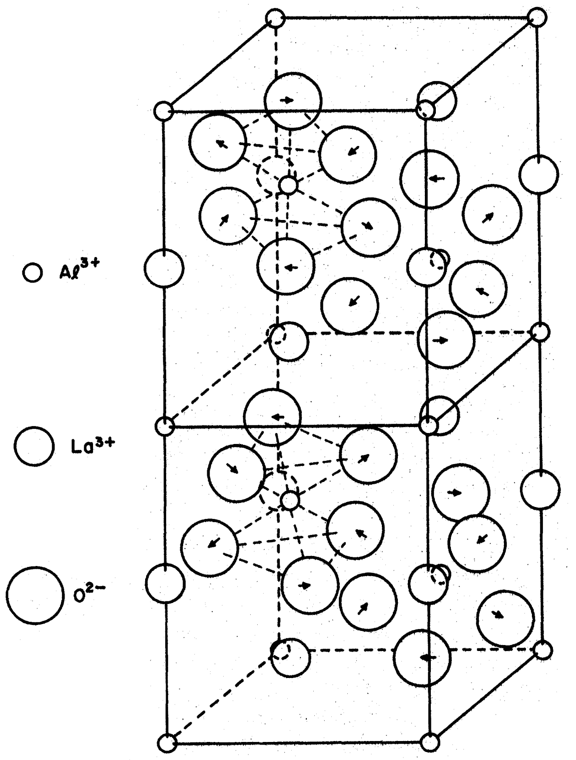

FIG. 1. Hexagonal primitive unit cell of $LaAlO_3$. The arrows show the rotation of the O^{2-} triangles in the rhombohedral phase.

Zonn[10,11] who found $J^{ab} = -99.5$ cm^{-1}. Since both values are incorrect, the analysis used to obtain the ground-state exchange as well as the singly excited pair splittings are described in some detail. The recently observed transitions in the ultraviolet to the doubly excited pair levels are discussed in Sec. IV.[12] This manifold consists of four states with $S=0$ and four with $S=1$. The splittings of these levels are calculated in Sec. V using Eq. (1). The resulting level diagrams of the nearest-neighbor pairs are discussed in Sec. VI.

II. CRYSTAL STRUCTURE AND PREPARATION

$LaAlO_3$ crystallizes in the cubic perovskite structure with the space group $Pm3m(O_h^1)$. At 808 °K the crystal undergoes a phase transition to a rhombohedral modification having the space group $R\bar{3}c$ (D_{3d}^6).[13-15] The triply primitive hexagonal cell of this structure is shown in Fig. 1. The La^{3+} ions are on the 6 *a* sites, the Al^{3+} ions, for which the Cr^{3+} ions substitute, are on the 6 *b* sites, and the O^{2-} ions are found on the 18 *e* sites.[16] The sites have C_3, C_{3i}, and C_2 point-group symmetry, respectively. This compares with the perovskite structure where the La^{3+} and Al^{3+} sites have tetragonal D_{4h} symmetry and the O^{2-} sites have the full O_h symmetry.

Figure 1 illustrates how the change in the crystal symmetry at the phase-transition results from a small rotation of the O^{2-} ions in planes perpendicular to the *c* axis. The undetermined site parameter *x* of the $R\bar{3}c$ group determines the magnitude of the rotation, and this quantity is identified with the order parameter of the phase transition.[17,18] Recently, Marezio *et al.* have found $x = 0.541$ at 300 °K from an x-ray refinement of the structure.[15] The two oxygen triangles making up the sixfold coordination of a given Al^{3+} site have the same sense of rotation, resulting in a C_{3i} symmetry of the Al^{3+} site. The sense of rotation of the AlO_6 groups alternates along the *c* axis thus resulting in two types of Al^{3+} sites which, however, for the purposes of the experiments described here, are equivalent.

The separations of the first three types of Al^{3+} neighbors and the angles the pair axes make with the *c* axis are given in Table I. In the cubic perovskite structure the nearest-neighbor $Al^{3+}-O^{2-}-Al^{3+}$ bond is linear, and the substitution of Cr^{3+} ions results in a strong antiferromagnetic superexchange. The situation is not appreciably changed in the distorted phase, since at room temperature the bond angle is 170.7°.[15] The orientation of a nearest-neighbor pair and the displacement of the oxygen ion is shown in Fig. 2. The coordinate frame of the perovskite cell is denoted by the *x*, *y*, and *z* axes. We define the coordinate frame of the pair having its *Z* axis along the perovskite [111] axis, and the *X* axis in the direction of the O^{2-} distortion. Thus the *x* and *y* perovskite axes make a 45° angle with the *YZ* plane and the *z* axis lies in this plane.

The more distant pairs involve a series of bonds, and the exchange coupling will correspondingly be much weaker. Hence only the first-nearest-neighbor pair will exhibit an appreciable exchange coupling.

An oriented single crystal grown by the Czochralski method and containing about 0.05-wt% Cr^{3+} was obtained from Union Carbide. The material as grown contained a number of twins resulting from trigonal distortions along the four ⟨111⟩ directions

TABLE I. Separation of the first three nearest-neighbor pairs based on a triply primitive hexagonal unit cell of $a = 5.365$ Å and $c = 13.11$ Å.[a]

Nearest-neighbor pair type	Number of neighbors	Angle with *c* axis	Separation	Number of ~180° bonds	Exchange
First	6	54.7°	3.79	1	AFM
Second	6 6	90° 35.3°	5.36	2	FM
Third	2 6	0° 70.3°	6.56	3	AFM

[a] S. Geller and V. B. Bala, Acta Cryst. 9, 1019 (1956).

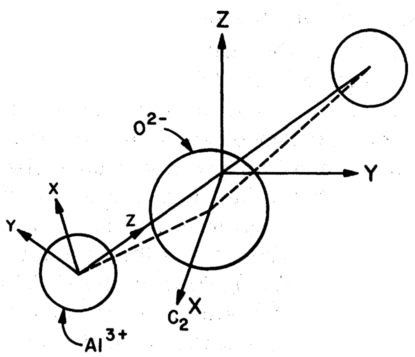

FIG. 2. Orientation of the nn Al^{3+} pair. The coordinate frames are discussed in the text.

of the perovskite cell. The crystal was detwinned by the method of Fay and Brandle.[19,20] The crystal easily retwins when stressed in other directions, either by an externally applied stress, or an internal stress resulting from rapid temperature cycling. A crystal with a 1.0-wt% Cr^{3+} concentration was grown by Brandle of the Bell Telephone Laboratories. Crystals with these high Cr^{3+} levels are more difficult to grow than with more dilute doping levels. Even though the boule was pulled at a speed of less than 0.2 cm per hour, the crystal contained numerous small inclusions. Consequently, it was not possible to detwin this sample completely.

The boules initially contained a color center which absorbed strongly in the blue, and gave the crystal a dark red color. This defect apparently results from the replacement of a La^{3+} ion by a Ca^{2+} impurity and a nearby hole.[20] The centers were bleached by heating for several hours at 1100 °C in a hydrogen atomosphere. The treated crystal had a light pink color typical of a dilute Cr^{3+} concentration. The bleaching process increased the emission intensity of single ions and pairs. In addition, a new broad red emission peaking at 6230 Å is observed which is tentatively identified with a Mn^{2+} impurity.

Although the ultraviolet (uv) absorption was only measurable in the bleached crystal, the uv excitation spectrum, described in Sec. IV, was obtained for both crystal conditions. Except for a change in intensity the two spectra are essentially identical, indicating the defect centers are not associated with Cr^{3+} pairs. Furthermore, excitation into the uv pair band did not recolor the crystal.

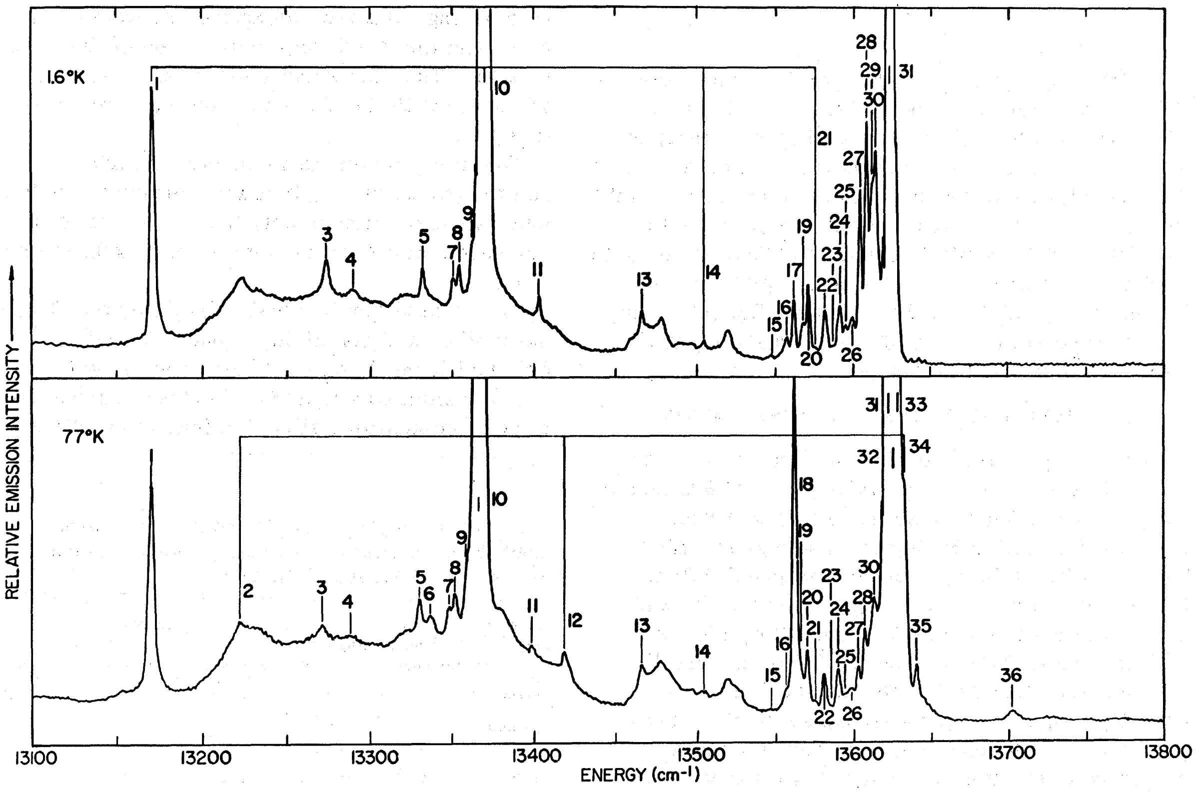

FIG. 3. Emission spectrum of Cr^{3+} single ions and pairs in $LaAlO_3$ at 1.6 and 77 °K. The energies of the numbered lines are listed in Table II.

TABLE II. Energy levels from Fig. 3.

Line from Fig. 2	ν (cm^{-1}) 1.6 °K	ν (cm^{-1}) 77 °K	Predominant polarization	$\frac{\delta E}{\delta p}\left(\frac{\text{cm}^{-1}\,\text{cm}^2}{\text{kg}}\right)$	Remarks
1	13171.9	13170.4	u	-0.0672 ± 0.003	$S=2\rightarrow3$
2	···	13223.4	π	-0.0682 ± 0.005	$S=1\rightarrow3$
3	13275.3	13272.0	π	-0.0611 ± 0.003	
4	13290.3	13288.0			
5	13331.9	13330.5	u		
6	···	13337.7	u		
7	13350.5	13348.4			
8	13353.8	13352.1			
9	13361.2	13359.1			
10	13368.5	13366.9	π	-0.0597 ± 0.003	$S=2\rightarrow2$
11	13402.2	13400.1		-0.0598 ± 0.003	
12	···	13419.6	π	$-0.063\ \pm0.003$	$S=1\rightarrow2$
13	13468.6	13466.3	π	-0.0686 ± 0.002	
14	13506.8	13505.4	π	-0.0566 ± 0.004	$S=2\rightarrow1$
15	13549.1	13545.9	π		
16	13558.9	13556.5			
17	13563.5	···			
18	···	13562.4	σ	-0.0624 ± 0.002	$S=1\rightarrow1$
19	13569.5	13566.7		-0.0578 ± 0.004	
20	13572.5	13570.3	u	-0.0447 ± 0.008	
21	13577.6	13574.9		-0.0578 ± 0.004	$S=2\rightarrow0$
22	13583.2	13581.0	u	-0.0302 ± 0.002 -0.0697 ± 0.003	
23	13588.2	13585.6			
24	13592.6	13590.1	u	-0.0161 ± 0.001 -0.0612 ± 0.001	
25	13596.5	13594.1			
26	13600.7	13598.3			
27	13605.4	13602.8	u	-0.0612 ± 0.004	
28	13609.2	13607.1	u	-0.0569 ± 0.005	
29	13613.0	13610.7			
30	13615.0	13613.2	u	-0.03925 ± 0.003	
31	13624.5	13623.1	MD	-0.0702 ± 0.004	$R1(^2E2\bar{A})$
32	13627.9	···		-0.0688 ± 0.004	
33	13269.9	13628.5	MD	-0.0322 ± 0.004	$R2(^2E\ \bar{E})$
34	···	13633.0			$S=1\rightarrow0$
35	···	13640.8	π		
36	···	13701.0	π	$-0.050\ \pm0.003$	$S=1\rightarrow1$

III. INFRARED SPECTRUM

A. Fluorescence

Figure 3 shows the emission from the annealed crystal at 1.6 and 77 °K obtained with a 1-m Czerny-Turner spectrometer and an S-20 response photomultiplier. There are several broad vibronic transitions at lower energies which do not apply to this work, and hence are not shown in Fig. 3.

The single-ion transitions at 77 °K are at 13 624.5 and 13 629.9 cm^{-1}, and the strongest pair line is at 13 366.9 cm^{-1} with somewhat weaker pair lines at 13 170.4 and 13 562.4 cm^{-1}. The analysis of the pair spectrum is complicated by the relatively strong R-line vibronics, and also the vibronics of the pairs. However, the pair transitions are substantially stronger for the more concentrated crystal. Furthermore, in Fig. 3 the intensity of the single-ion transitions and associated vibronics has been substantially reduced, relative to the pair fluorescence, by exciting into the uv pair band using the 3663.28-Å radiation from a high pressure 500-W Hg lamp. The significant emission lines of Fig. 3 are numbered and the corresponding energies are listed in Table II. The transitions from two of the excited states to the exchange-split ground-state levels, as determined below, are also shown in Fig. 3.

The pair spectrum intensity was enhanced by at least a factor 10, indicating that energy transfer from a doubly excited pair to the single ions is relatively unimportant at liquid-helium temperature. The enhancement is reduced at higher temperatures, for example, to a factor of 2.5 at CO_2 temperature (194.6 °K), because the higher-energy singly excited pair levels become thermally populated and the transfer from these levels to the single-ion ^2E_g levels is a nearly resonant process.

Polarization measurements indicate that the R lines are magnetic dipole. The relative intensities agree with the selection rules for C_{3i} site symmetry if the $2\bar{A}$ levels of ^2E_g are assumed to lie below $\bar{E}$. Thus the sign of the ^2E_g splittings is the same as for the emerald and spinel, but opposite to that for ruby. In a number of cases the pair lines had nearly equal intensity in σ and π polarizations, and the dipole nature could not be identified. These are labeled u in Table II. Several other pair lines are at least partially polarized. In particular, line 18 appears only in σ and α polarizations. A comparison with the axial spectrum showed these lines to be electric dipole. The dominant polarization of the lines is listed in Table II.

B. Temperature Dependence of Emission

The temperature dependences of several of the more prominent transitions are plotted in Fig. 4 as a function of T^{-1}. For these measurements the crystal was attached to a copper block and the temperature was measured using copper-vs-constantan and gold-iron-vs-chromel thermocouples. Excitation into the $^4T_{1g}$ band (4000–4500 Å) was used. The peak rather than the integrated intensities are shown. This does not lead to serious discrepancies for $T < 77$ °K since below this temperature the linewidths are relatively constant. Furthermore, for the sharper lines a wide spectral slit width was used. The peak height then closely corresponds to the integrated intensity.

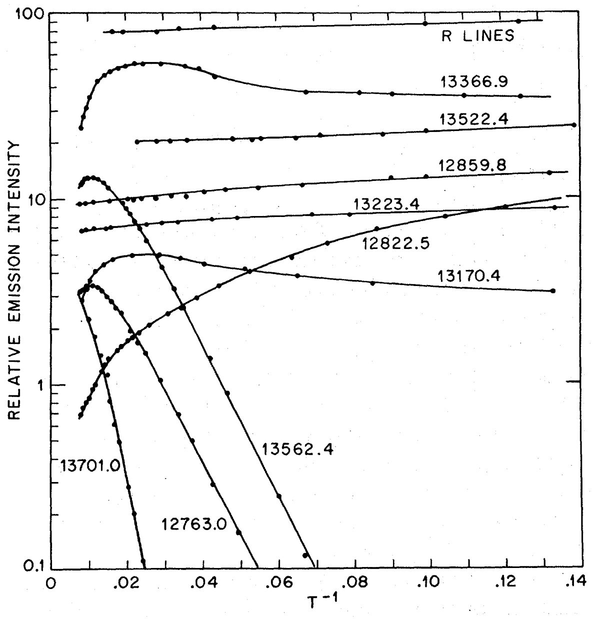

FIG. 4. Relative emission intensities of some of the lines of Fig. 3 plotted as a function of T^{-1}.

The following conclusions are drawn from Fig. 4:

(i) The single-ion fluorescence decreases slowly with increasing temperature and the similar dependence of the lines at 13 522.4, 12 972.8 (not shown in Figs. 3 and 4), and 12 859.8 cm^{-1} identify these lines as vibronics of the R lines. This agrees with the relative emission intensities obtained for single and pair excitations. Tkachuk and Zonn had identified the line at 12 859.8 cm^{-1} as the transition to the $S = 3$ ground-state level of the nearest-neighbor (nn) pair.[10] Our temperature dependence rules out this assignment. Up to 50 °K the 13 223.4-cm^{-1} transition has a temperature dependence characteristic of an R-line vibronic; however, additional structure appears at higher temperatures. This emission is identified as a superposition of a broad R-line vibronic and a sharper pair transition which has the same initial level as the 13 562.4-cm^{-1} emission.

(ii) The similar dependences of the 13 366.9- and 13 170.3-cm^{-1} emission indicate these transitions belong to the same pair system and originate from the lowest level of the singly excited pair.

(iii) The 12 822.5-cm^{-1} emission has the same dependence as the 13 607.1- and 13 602.8-cm^{-1} lines (not shown in Fig. 4) which are transitions of more distant pairs. This transition is identified as a vibronic of the latter lines.

(iv) The dependence of the 13 562.4-cm^{-1} emission indicates that the line originates on a level of the singly excited pair whose energy as deduced from the slope at low temperatures is ≈ 60 cm^{-1} above the lowest level. The 12 763-cm^{-1} emission is a vibronic of this line.

(v) Line 36 at 13 701 cm^{-1} originates on a still higher energy pair state, which from its temperature dependence is about 170 cm^{-1} above the lowest level.

We show in Sec. V that the electric dipole $\Delta S = 0$ transitions to two of the $S = 1$ states and two of the $S = 2$ states are expected to be large while the transitions to the remaining four excited states have weak dipole strengths. Three of these strong transitions have been observed in emission and it remains to find the fourth as well as to correlate the terminal levels of the transitions with levels of the exchange-split ground state, and to determine the spin values and energies of the levels.

C. Absorption Spectrum

The most conclusive technique of identifying the ground-state levels of an exchange-split pair is to

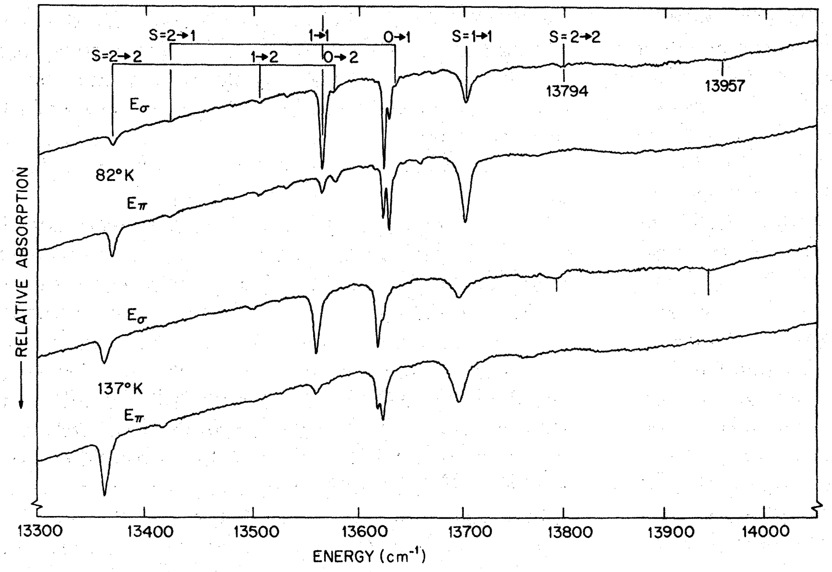

FIG. 5. Polarized absorption spectrum at 82 and 137 °K.

measure the temperature dependence of the absorption. For a given pair the population of a state with spin S and energy $E(S)$, obtained from Eq. (1), is

$$P(S)=(2S+1)e^{-E(S)/kT}/\textstyle\sum_{S'}(2S'+1)e^{-E(S')/kT}. \quad (4)$$

Figure 5 shows the polarized absorption spectrum at 82 and 137 °K. In addition to the R lines, strong absorption corresponding to lines 10, 18, and 36 in emission are observed, as well as two new lines at 13 794 and 13 957 cm^{-1} which appear in σ and α polarizations. However, absorption corresponding to line 1 is absent, hence this emission line terminates

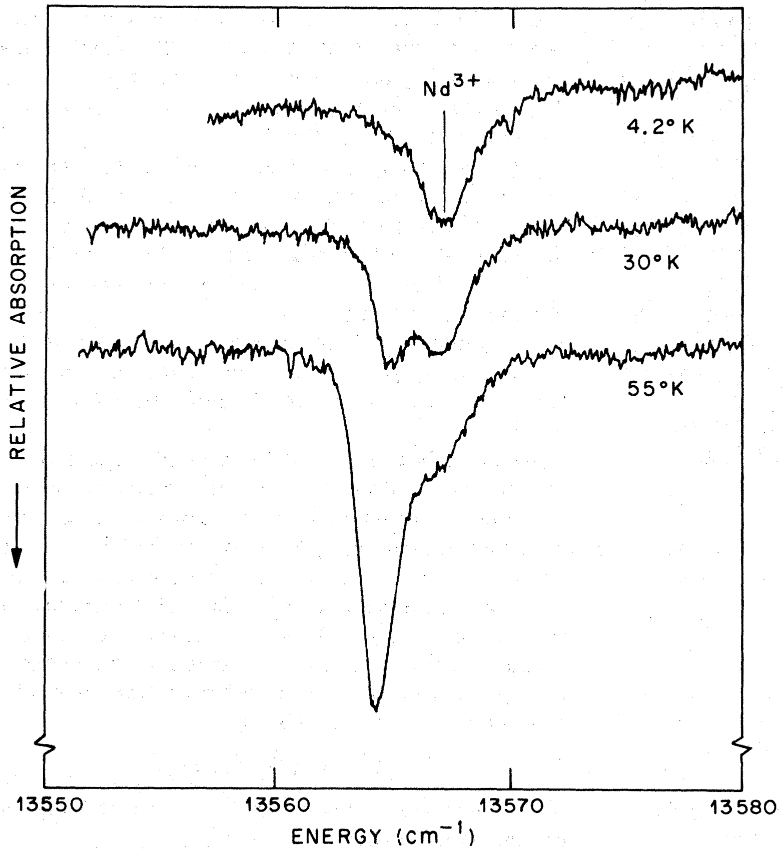

FIG. 6. Absorption spectrum of line 18 at several temperatures. A weak line due to an inadvertent Nd^{3+} impurity is also present.

on a higher energy, thermally unpopulated, ground-state level. The strong pair absorption vanishes at low temperatures; for example, Fig. 6 shows the evolution of line 18 with temperature. The absorption of lines 18 and 36 have a weaker dependence on temperature than line 10 and the 13 794- and 13 957-cm^{-1} lines, and the latter transitions originate on a higher-energy ground-state level than the former lines. The integrated absorption coefficients measured in relative units are listed in Table III. The 1% Cr^{3+} crystal used to obtain Fig. 5 contained a number of inclusions and defects which prevented the complete detwinning of the crystal. Hence the spectrum is partially depolarized, and for a given transition this introduced an error estimated to be equal to 20% of the difference in the absorption coefficients for the two polarizations. Measurements on the 0.05% sample showed that the 13 562.4-, 13 794-, and 13 957-cm^{-1} lines appear only in σ and α polarizations.

These results lead to the identification of the exchange-split ground-state manifold for the transitions from two of the excited pair states which are indicated in Fig. 3 and the transitions are listed in Table II. The spin values involved in the pair absorption are also shown in Fig. 5. The ground-state exchange splittings deduced from this analysis are listed in Table IV, and substituting into Eq. (2) yields $J = -66.6\ \text{cm}^{-1}$ and $j = -0.76\ \text{cm}^{-1}$.

The curves of Fig. 7 show the calculated populations of the $S = 1$ and 2 pair levels, plotted as a function of T^{-1}, and were obtained using the values of $E(S)$ in Table IV. The solid points are the measured integrated absorption coefficients of lines 10 and 18, which were multiplied by constants in order to superimpose them on the level population curves. The excellent agreement provides convincing confirmation of the ground-state exchange splitting and the identification of the spin values of the singly excited states. The nn pair transitions listed in Table II are shown in the energy-level diagram Fig. 8.

It is of some interest to compare the value of the exchange of the pairs with the exchange of the concentrated material LaCrO_3. There are several approximations which relate the magnetic data to the exchange parameter. A reasonably accurate value is obtained from the Curie-Weiss temperature θ.[21,22] Considering only the nn exchange with the six neighbors, we have

$$J = -k\theta/2S(S+1) .$$

Using the Néel temperature of 320 °K,[23,24] and the ratio $\theta/T_N = 1.78$, obtained from susceptibility measurements from $2T_N < T < 3T_N$, we obtain $J = -52.7$ cm^{-1}. The series-expansion method of Rushbrooke and Wood[25] yields a direct relationship between the

TABLE III. Integrated absorption coefficients, in relative units, of the nearest-neighbor pair spectrum shown in Fig. 4.

	82 °K		137 °K	
ν	σ	π	σ	π
13 366.9	1.07	2.36	2.68	6.1
13 562.4	5.7	1.1	5.5	1.1
13 701	3.75	8.0	3.45	7.3
13 794	0.45	···	1.1	···
13 957	0.11	···	3.1	···

TABLE IV. Ground-state exchange splittings of the nearest-neighbor pairs.

	1.6 °K	77 °K		Calc[a]
S	$\Delta\nu_{S,S-1}$	$\Delta\nu_{S,S-1}$[b]	$\Delta\nu_{S,S-1}$[c]	$\Delta\nu_{S,S-1}$
1	70.8	69.5	70.6	71.5
2	138.3	138.5	142.8	138.5
3	196.6	196.5	196.2	196.4

[a] Using $J = -66.6\ \text{cm}^{-1}$, $j = -0.76\ \text{cm}^{-1}$.
[b] From $S = 2$ excited state.
[c] From $S = 1$ excited state.

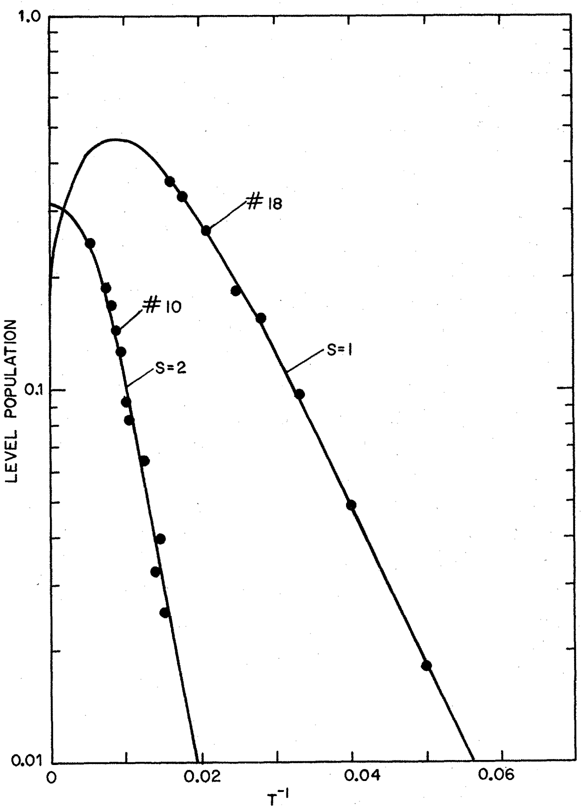

FIG. 7. The curves are the level populations for $S = 1$ and 2 calculated using Eq. (4) and the data of Table IV. The solid points are the integrated absorption coefficients of lines 10 and 18.

exchange and T_N, which for $S=\frac{3}{2}$ reduces to[22]

$$J=-0.197T_N .$$

Substituting for T_N we obtain $J=-43.8\ \mathrm{cm}^{-1}$. The calculated values are somewhat smaller than the measured exchange parameter of the pair. A similar result was obtained for ruby pairs and Cr_2O_3 by Mollenauer and Schawlow[1,26] who computed $\theta=875\ ^\circ\mathrm{K}$ using the pair exchange values. This is about 50% larger than the measured Cr_2O_3 θ of $(550\pm20)\ ^\circ\mathrm{K}$.

D. Effects of Uniaxial Stress

Previous studies of the ruby pair spectrum show the pair lines to shift remarkably under the application of a uniaxial stress, and this yields important information concerning the type of pair responsible for the emission.[26-28] In particular, Mollenauer investigated the angular stress dependence of several ruby pair emission lines. When the stress is in a general direction the equivalence of the sites, which are equivalent in zero stress, is destroyed. The shift of the emission depends on the angle between the axis of the pair and the direction of the stress, and the unequal shifts from inequivalent sites result in a pseudosplitting of the emission line.

Due to the susceptibility to twinning it has proved to be unfeasible to study the angular stress dependence of the emission lines. However, because of the simplicity of the pair system most of the required information can be obtained from measurements of the shift of the emission with stresses applied parallel to the trigonal axis. Examination of Fig. 1 shows the first nn to remain equivalent to the trigonal stress. The second- and the third-nn sites become inequivalent and the ratios of the sites are 6 : 6 and 2 : 6, respectively. Hence the emission from nn pairs will only shift, while the emission from second- and third-nn pairs will exhibit a pseudosplitting as well as a shift of the center of gravity. Furthermore, the relative intensities of the split components of an emission line are determined by the level populations. Thus in principle the intensity ratios could be used to identify the second- and third-neighbor emission.

The measurements were made at 1.6 and 77 °K using the stress apparatus previously used by Sturge.[29] The samples were oriented and detwinned rectangular prisms of approximately 2.45-mm^2 cross section. Consistent results were obtained using samples having different areas. Stresses up to 45 kg/mm^2 were regularly applied. Since only a limited number of samples were available, no attempt was made to determine the ultimate elastic strength of the material.

The stress dependences obtained from a least-squares fit to the experimental data are given in the fifth column of Table II. All lines shift to lower energy with increasing stress and although in general the shifts of the pair lines are the same order as the shift of $R1$, there is a definite dependence on the final pair state. This is shown in Fig. 9 in which we plot the stress parameters as a function of the ground-state exchange energy for the transitions from the $S=2$ and 1 excited states. The stress parameter for the $S=2$ data varies as 0.0017 $\mathrm{cm}^{-1}\,\mathrm{kg}^{-1}\mathrm{mm}^2$ per unit of J. This is the stress dependence of the ground-state exchange. The less complete data for the first $S=1$ state have a qualitatively similar dependence on the ground-state exchange, but compared with the $S=2$ data the shift is larger. The one data point from the second $S=1$ level indicates that the stress dependence from this level is smaller than from the $S=2$ level. The dependence on ground-state energy confirms the intuitive assumption that compression increases the overlap and hence results in a larger exchange interaction. The significance of the above number is not readily apparent, however as the direction of stress makes an ≈54.7° angle with the pair axis, and the net shift results from the effect of stress both parallel and perpendicular to the pair axis.

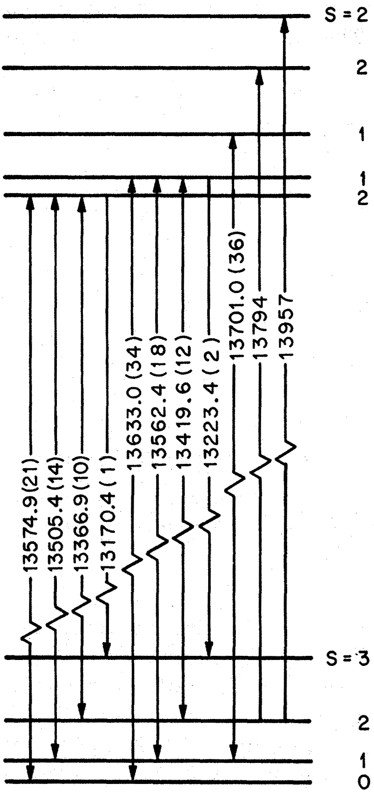

FIG. 8. The energy levels and spin values of the nn pair.

The first-nn shifts are considerably smaller than found for ruby.[26] Mollenauer found the first-nn line at 7540 Å to shift +0.025 $\mathrm{cm}^{-1}\,\mathrm{kg}^{-1}\,\mathrm{mm}^2$, and the 7302 Å first-nn line exhibits a shift of about

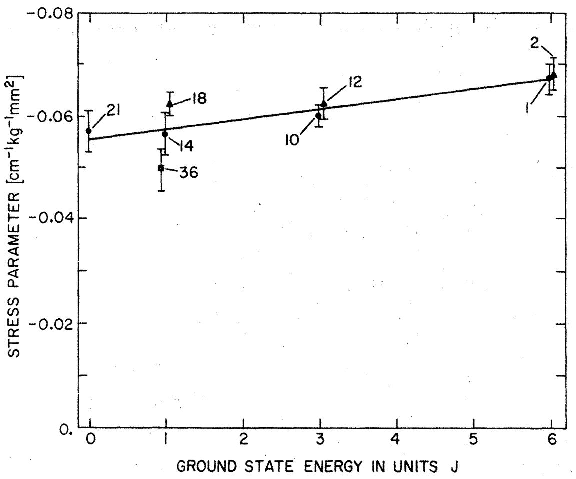

FIG. 9. The stress parameters of the nn pair lines plotted as a function of the ground-state energy.

one-half this value. The approximately six times larger shift in ruby, as well as the change in sign, is apparently related to the different orientation of the oxygen ions.

Pseudosplittings were resolved for two of the more intense lines near 13 600 cm^{-1}. Due to intensity limitations the splittings of a number of weaker lines could not be resolved. For these the average shift was measured.

E. Magnetic Field Dependence

The polarized emission spectrum was examined in fields up to 50 kOe using a superconducting solenoid. The single-ion spectrum yields $g_{\parallel}(^4A_2) = 2.005 \pm 0.03$ and $g_{\parallel}(2\bar{A}) = 1.795 \pm 0.03$ from the $R1$ data and $g_{\parallel}(^4A_2) = 1.996 \pm 0.03$ and $g_{\parallel}(\bar{E}) = -2.010 \pm 0.03$ from $R2$. The ground-state g values agree with $g_{\parallel}(^4A_2) = 1.9825 \pm 0.0005$ obtained by Kiro, Low, and Zusman from electron-spin-resonance measurements.[30]

Line 10 does not split in a magnetic field. Rather the full width at half-maximum decreases from 2.7 cm^{-1} in zero field to 2.0 cm^{-1} at 50 kOe. It is apparent from the asymmetrical line shape that the zero-field emission consists of several unresolved components from transitions between the crystal-field split levels of the two $S = 2$ states. We expect the g values of the initial and final pair states to be approximately equal as the g values of the single-ion states making up the pair are not very different. Hence, as is observed, when the magnetic field splittings are large compared to the zero-field splittings, the linewidth will be smaller and the line shape will be more symmetrical. An upper bound on the difference between the pair g factors of 0.1 is obtained by attributing at most 1 cm^{-1} of the linewidth to this origin at 50 kOe. Thus, both the absence of a splitting and the line narrowing imply that the selection rule $\Delta M_s = 0$ applies quite rigorously to this transition. This result, in addition to the rule $\Delta S = 0$ obtained from Fig. 3 and the electric dipole nature of the emission, indicates that the major part of the pair transition is due to the exchange-induced electric dipole mechanism initially proposed for the magnon sidebands in antiferromagnets by Tanabe *et al.*[31]

The magnetic field splits line 1 into three components. The splittings correspond to $g_{\parallel} = 2.03$ and $g_{\perp} = 1.81$ for $\vec{H}$ parallel and perpendicular to the c axis, respectively, and indicates that the two outermost components are $\Delta M_s = \pm 1$ transitions and the central component has $\Delta M_s = 0$. Since $\Delta S = \pm 1$, this is a "forbidden" transition in the sense that it does not simply obtain its intensity from the exchange-induced dipole moment mechanism. This pair line is appreciably stronger than the two remaining "forbidden" transitions, to $S = 1$ and 0. We attribute its intensity to higher-order exchange processes and to magnetic dipole transitions of the two coupled ions.

IV. ULTRAVIOLET SPECTRUM

The absorption at approximately twice the ^2E - $^4A_2$ separation, shown in Fig. 10, has already been identified with the simultaneous excitation of *both* ions of the pair to the ^2E states.[12] The low-temperature absorption was shown to originate on the $S = 0$ ground-state pair level. The absorption which appears at high temperature, denoted in Fig. 10 by an asterisk, has a temperature-dependence characteristic of the $S = 1$ ground-state pair level population.

The low-temperature absorption at 26 706 and 27 758 cm^{-1} appears in σ and α polarizations, and the 27 343-cm^{-1} absorption appears most strongly in π polarization. The $S = 1$ line at 27 063 cm^{-1} is also σ and α polarized.

The remaining electronic transitions are either too weak to be identified, or are superimposed on the vibronics. As examples of the latter, the weak 27 406-cm^{-1} absorption is mainly π polarized at low temperatures, indicating it is a vibronic of the 27 337-cm^{-1} absorption. However, at higher temperatures the absorption appears most strongly in σ polarization, and this new absorption is tentatively identified with an $S = 1$ electronic transition. Similarly the line at 27 457 cm^{-1} is a vibronic of the 26 701 cm^{-1} absorption. At higher temperatures a predominantly π-polarized transition is superimposed on this line, which is also tentatively identified as an $S = 1$ electronic transition.

Thus, six of the eight pair levels have been identified. The electronic lines and the origin of the strong vibronics are discussed in greater detail in Sec. VI.

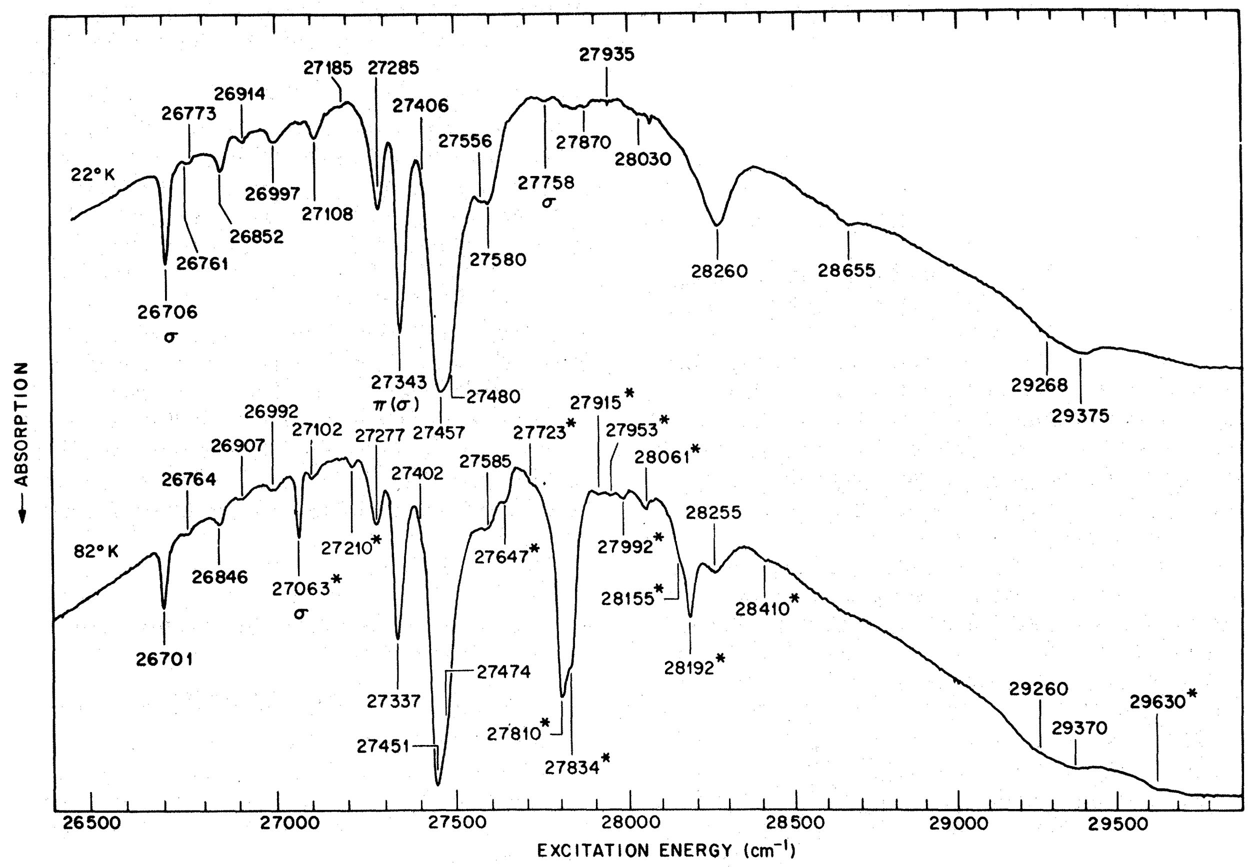

FIG. 10. Absorption spectrum resulting from the excitation of both ions of the pair to the ^2E states. The electronic transitions, as determined from the polarization, are labeled σ and $\pi(\sigma)$. The transitions from the $S=1$ level are denoted by an asterisk.

The strong lines do not split for magnetic fields up to 50 kOe along the trigonal crystal axis. This implies the selection rule $\Delta M_s = 0$ and, with the $\Delta S = 0$ selection rule obtained from Fig. 10, indicates that these transitions also obtain their dipole strength from the exchange-induced electric dipole moment.[31]

The excitation spectrum of the pair fluorescence is shown in Fig. 11. Either a small Bausch and Lomb spectrometer or a set of appropriate Corning glass filters was inserted in front of the photomultiplier to isolate the pair emission at 13 367 cm^{-1}. With the Bausch and Lomb spectrometer tuned to the R-line emission, the structure of Fig. 11 was not observed at low temperatures, although the background corresponding to the high-energy vibronic tail of the $^4A_{2g} \rightarrow {}^4T_{1g}$ transition was intensified.

The preferential excitation of the pair emission was used in Sec. III A to separate the infrared pair transitions from the single-ion vibronic spectrum. This was particularly successful because the pressure-broadened 3663.28-Å (27 290-cm^{-1}) Hg emission overlaps the strongest pair absorption lines. The absence of single-ion emission at low temperatures indicates that the $^2E\,^2E \rightarrow {}^2E\,^4A_2$ decay rate of the pair greatly predominates over the transfer of energy from the doubly excited pair to the nearby "single" ions.

V. THEORY OF THE NEAREST-NEIGHBOR PAIR

A. Energy Levels

The theory of the exchange interaction of ion pairs in the $(t_{2g})^3$ configuration based on the single electron-electron exchange of Eq. (1) has recently been developed by Huang and by Pryce.[7,8] Their results are used in this section to compute the nearest-neighbor exchange splitting in terms of the empirical parameters J_{ij}. We define the t_{2g} wave functions in the perovskite (x, y, z) coordinate frame (Fig. 2). The three orbital functions $|\xi\rangle$, $|\eta\rangle$, and $|\zeta\rangle$ have angular dependences proportional to yz, zx, and xy, respectively, and the $M_s = +\frac{1}{2}(-\frac{1}{2})$ spin state of an electron in the ξ orbital is denoted by $|\xi\rangle$ ($|\bar{\xi}\rangle$). For the i, j subscripts of J_{ij} we further introduce the indices 1, 2, and 3 to denote the orbitals $|\xi\rangle$, $|\eta\rangle$, $|\zeta\rangle$, respectively.

In the cubic coordinate frame the ${}^4A_{2g}$ and ${}^2E_g$ wave functions, quantized along the z axis, are

$$\begin{aligned} A_{3/2} &= |\xi\eta\zeta|, \\ E_{\theta,1/2} &= (1/\sqrt{2})(|\xi\bar{\eta}\zeta| - |\bar{\xi}\eta\zeta|), \\ E_{\epsilon,1/2} &= (1/\sqrt{6})(2|\xi\eta\bar{\zeta}| - |\xi\bar{\eta}\zeta| - |\bar{\xi}\eta\zeta|), \end{aligned} \tag{5}$$

where $|\xi\eta\zeta|$ is the normalized Slater determinental wave function and the subscripts denote the component of M_s. The single-ion site actually has C_{3i} symmetry, and the appropriate ${}^2E_g$ wave functions quantized along the trigonal axis are easily obtained by an Eulerian angle transformation. However, for the analysis of the pair system it is more convenient to retain the wave functions defined by Eq. (5). The energies are independent of the axis of quantization.

In the undistorted perovskite structure the nearest-neighbor pair has tetragonal (D_{4h}) symmetry and the bond axis is taken to be the z direction. The application of the symmetry operations leads to four inequivalent exchange parameters:

$$J_{11}=J_{22},\quad J_{33},\quad J_{12}=J_{21},\quad J_{13}=J_{23}=J_{31}=J_{32}. \tag{6}$$

The question of the relative magnitudes of the J_{ij} has been discussed by Anderson.[32] The results of his theory show that for the case of a linear Cr^{3+}—O^{2-}—Cr^{3+} bond the J_{11} terms are dominant and derive their magnitude from the kinetic exchange

$$J_{11} = -(b_\pi)^2/U, \tag{7}$$

where b_π is the transfer integral representing the effect of kinetic energy causing the electrons to move through the lattice via the bonding of the d_{xz} (d_{yz}) Cr^{3+} orbitals with the O^{2-} P_x (P_y) π orbitals. U is the repulsive average electrostatic energy which results when both electrons are on the same ion. There is also a ferromagnetic potential exchange interaction

$$J_{12} = J_\pi, \tag{8}$$

where J_π is a measure of the repulsive interelec-

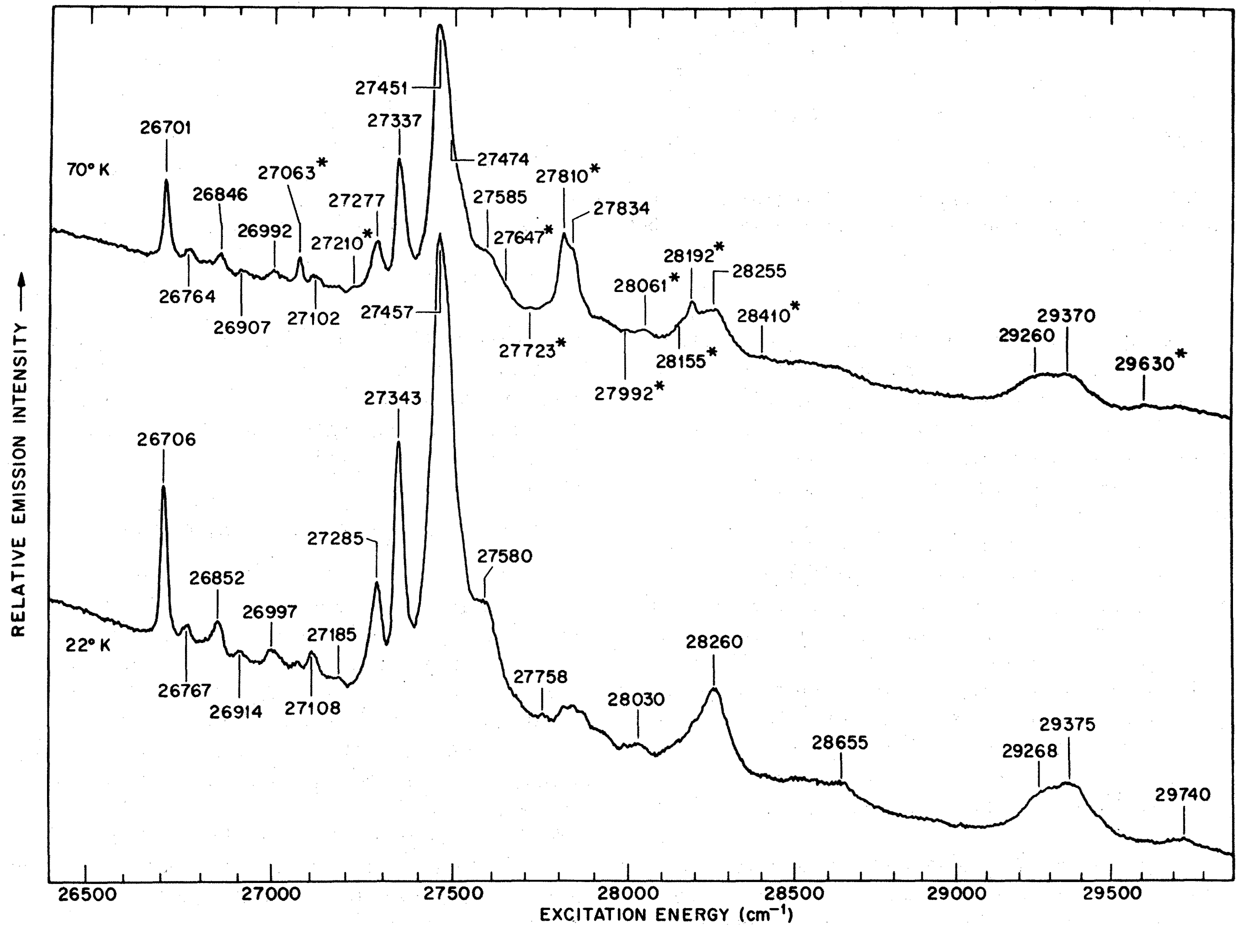

FIG. 11. Excitation spectrum of the pair emission (predominantly the $S=2\rightarrow 2$ transition at 13 367 cm^{-1}) corresponding to the absorption spectrum of Fig. 9.

tronic potential energy. Anderson further argues that the remaining exchange terms will be small. However, for the sake of completeness we shall include all the parameters in this section, and then simplify the results in the next section.

For the C_2 symmetry of the actual pair we obtain six parameters:

$$J_{11}=J_{22}=A,\quad J_{33}=B,\quad J_{12}=C',$$
$$J_{21}=C'',\quad J_{13}=J_{32}=D',\quad J_{31}=J_{23}=D'' . \tag{9}$$

Since the distortion from tetragonal symmetry is relatively small the exchange parameters for the two symmetries are expected to be nearly equal. We thus expect $J_{12}\approx J_{21}$ and $J_{13}\approx J_{31}$ and let

$$C'=C+E,\quad C''=C-E ,$$
$$D'=D+F,\quad D''=D-F , \tag{10}$$

where E and F are small quantities. Furthermore, using the wave functions which diagonalize the exchange Hamiltonian for tetragonal symmetry, the terms containing E and F are found to appear only on the off-diagonal parts of the matrix. Hence, in the lowest-order approximation the exchange parameters effectively have the tetragonal symmetry of the ideal perovskite pair.

For a given S value the exchange Hamiltonian has off-diagonal matrix elements between the ground, singly excited, and doubly excited pair states. As shown in Sec. VB, these are crucial to the existence of the exchange-induced dipole moment. However, since the energies of the levels differ by the single-ion ${}^2E_g$ energy, the off-diagonal terms make small contributions to the energies, and are neglected in the following calculations. Except for four levels of the doubly excited pair, the symmetric and antisymmetric combinations of the excited-state wave functions diagonalize the large contributions of $\mathcal{H}_{ex}$. Neglecting the small off-diagonal terms then yields the energy levels directly.

1. *Ground-State Pair States*

In terms of the parameters of Eq. (9) the ground-state exchange is

$$J^{ab}=\tfrac{1}{9}[2(A+C)+B+4D]. \tag{11}$$

The wave functions of these levels are

$$|{}^4A_2,\ {}^4A_2;\ S=3,\ M_s=3+\rangle=A^a_{3/2}A^b_{3/2}\ ,$$

$$|{}^4A_2,\ {}^4A_2;\ S=2,\ M_s=2-\rangle$$
$$=(\sqrt{\tfrac{1}{2}})(A^a_{3/2}A^b_{1/2}-A^a_{1/2}A^b_{3/2}),$$

$$|{}^4A_2,\ {}^4A_2;\ S=1,\ M_s=1+\rangle$$
$$=(\sqrt{\tfrac{3}{10}})\ (A^a_{3/2}A^b_{-1/2}+A^a_{-1/2}A^b_{3/2})-(\sqrt{\tfrac{2}{5}})A^a_{1/2}A^b_{1/2}\ ,$$

$$|{}^4A_2,\ {}^4A_2;\ S=0,\ M_s=0-\rangle$$
$$=\tfrac{1}{2}(A^a_{3/2}A^b_{-3/2}-A^a_{-3/2}A^b_{3/2}+A^a_{-1/2}A^b_{1/2}-A^a_{1/2}A^b_{1/2}), \tag{12}$$

where the A_{M_s} single-ion functions are given by Eq. (5). The parity of the wave functions under interchange of the ions is denoted by the + and − in the kets.

2. *Singly Excited Pair States*

The wave functions of the $S=1$, $M_s=1$ pair levels are

$$|a+\rangle=\frac{1}{2\sqrt{2}}\,[\sqrt{3}\ (E^a_{\theta,-1/2}A^b_{3/2}+A^a_{3/2}E^b_{\theta,-1/2})$$
$$-(E^a_{\theta,1/2}A^b_{1/2}+A^a_{1/2}E^b_{\theta,1/2})]\ ,$$
$$|a-\rangle=\frac{1}{2\sqrt{2}}\,[\sqrt{3}\ (E^a_{\theta,-1/2}A^b_{3/2}-A^a_{3/2}E^b_{\theta,-1/2})$$
$$-(E^a_{\theta,1/2}A^b_{1/2}-A^a_{1/2}E^b_{\theta,1/2})]\ , \tag{13}$$
$$|b+\rangle=\frac{1}{2\sqrt{2}}\,[\sqrt{3}\ (E^a_{\epsilon,-1/2}A^b_{3/2}+A^a_{3/2}E^b_{\epsilon,-1/2})$$
$$-(E^a_{\epsilon,1/2}A^b_{1/2}+A^a_{1/2}E^b_{\epsilon,1/2})],$$
$$|b-\rangle=\frac{1}{2\sqrt{2}}\,[\sqrt{3}\ (E^a_{\epsilon,-1/2}A^b_{3/2}-A^a_{3/2}E^b_{\epsilon,-1/2})$$
$$-(E^a_{\epsilon,1/2}A^b_{1/2}-A^a_{1/2}E^b_{\epsilon,1/2})],$$

and yield the diagonal matrix elements of $\mathcal{H}_{ex}$,

$$\langle a+|\mathcal{H}_{ex}|a+\rangle=R+\tfrac{1}{12}[2(A-C)+5(B+2D)]\ ,$$
$$\langle a-|\mathcal{H}_{ex}|a-\rangle=R+\tfrac{1}{4}[2(A+C)-(B-2D)]\ ,$$
$$\langle b+|\mathcal{H}_{ex}|b+\rangle=R+\tfrac{1}{36}[22(A+C)-(B-2D)], \tag{14}$$
$$\langle b-|\mathcal{H}_{ex}|b-\rangle=R+\tfrac{1}{12}[-2(A-C)+5(B+2D)]\ .$$

The nonzero off-diagonal elements are

$$\langle a+|\mathcal{H}_{ex}|b-\rangle=-(2E+F)/2\sqrt{3}\ ,$$
$$\langle a-|\mathcal{H}_{ex}|b+\rangle=-(4E+7F)/6\sqrt{3}\ . \tag{15}$$

Similarly, the $S=2$, $M_s=2$ wave functions are

$$|c+\rangle=\frac{1}{\sqrt{2}}\,(E^a_{\theta,1/2}A^b_{3/2}+A^a_{3/2}E^b_{\theta,1/2}),$$
$$|c-\rangle=\frac{1}{\sqrt{2}}\,(E^a_{\theta,1/2}A^b_{3/2}-A^a_{3/2}E^b_{\theta,1/2})\ ,$$
$$|d+\rangle=\frac{1}{\sqrt{2}}\,(E^a_{\epsilon,1/2}A^b_{3/2}+A^a_{3/2}E^b_{\epsilon,1/2})\ , \tag{16}$$
$$|d-\rangle=\frac{1}{\sqrt{2}}\,(E^a_{\epsilon,1/2}A^b_{3/2}-A^a_{3/2}E^b_{\epsilon,1/2})\ .$$

The diagonal matrix elements of $\mathcal{H}_{ex}$ for $S=2$ are

$$\langle c+|\mathcal{H}_{ex}|c+\rangle=R+\tfrac{1}{4}[-2(A-C)-(B+2D)]\ ,$$
$$\langle c-|\mathcal{H}_{ex}|c-\rangle=R+\tfrac{1}{4}[2(A-C)-(B+2D)]\ ,$$

$$\begin{aligned}&\langle d+|\mathcal{H}_{\mathrm{ex}}|d+\rangle R+\tfrac{1}{4}[-2(A+C)-(B-2D)]\,,\\&\langle d-|\mathcal{H}_{\mathrm{ex}}|d-\rangle=R+\tfrac{1}{12}[-2(A+C)+5(B-2D)]\,.\end{aligned}\tag{17}$$

The nonzero off-diagonal elements are

$$\begin{aligned}&\langle c+|\mathcal{H}_{\mathrm{ex}}|d-\rangle=(2E-F)/2\sqrt{3}\,,\\&\langle c-|\mathcal{H}_{\mathrm{ex}}|d+\rangle=(\sqrt{3}/2)F\,.\end{aligned}\tag{18}$$

3. *Doubly Excited Pair States*

The $S=0$, $M_s=0$ wave functions are

$$\begin{aligned}|e-\rangle&=\frac{1}{\sqrt{2}}(E^a_{\theta,1/2}E^b_{\theta,-1/2}-E^a_{\theta,-1/2}E^b_{\theta,1/2})\,,\\|f-\rangle&=\frac{1}{\sqrt{2}}(E^a_{\epsilon,1/2}E^b_{\epsilon,-1/2}-E^a_{\epsilon,-1/2}E^b_{\epsilon,1/2})\,,\\|g+\rangle&=\tfrac{1}{2}(E^a_{\epsilon,1/2}E^b_{\theta,-1/2}+E^a_{\theta,-1/2}E^b_{\epsilon,1/2}\\&\qquad-E^a_{\epsilon,-1/2}E^b_{\theta,1/2}-E^a_{\theta,1/2}E^b_{\epsilon,-1/2})\,,\\|g-\rangle&=\tfrac{1}{2}(E^a_{\epsilon,1/2}E^b_{\theta,-1/2}-E^a_{\theta,-1/2}E^b_{\epsilon,1/2}\\&\qquad-E^a_{\epsilon,-1/2}E^b_{\theta,1/2}+E^a_{\theta,1/2}E^b_{\epsilon,-1/2})\,.\end{aligned}\tag{19}$$

The diagonal matrix elements of $\mathcal{H}_{\mathrm{ex}}$ are

$$\begin{aligned}&\langle e-|\mathcal{H}_{\mathrm{ex}}|e-\rangle=2R+\tfrac{3}{4}B\,,\\&\langle f-|\mathcal{H}_{\mathrm{ex}}|f-\rangle=2R+\tfrac{1}{12}[8(A+C)+(B-8D)]\,,\\&\langle g+|\mathcal{H}_{\mathrm{ex}}|g+\rangle=2R+\tfrac{1}{4}[-2(A-C)-(B-4D)]\,,\\&\langle g-|\mathcal{H}_{\mathrm{ex}}|g-\rangle=2R+\tfrac{1}{4}[2(A-C)-(B-4D)]\,.\end{aligned}\tag{20}$$

The off-diagonal matrix element between the $|e-\rangle$ and $|f-\rangle$ states now is large,

$$\langle f-|\mathcal{H}_{\mathrm{ex}}|e-\rangle=(A-C)/2\,,\tag{21}$$

and the energies of the admixed states $|e-\rangle$ and $|f-\rangle$ are

$$\begin{aligned}E=2R&+\tfrac{1}{12}[4(A+C)+(5B-4D)]\\&\pm\tfrac{1}{2}\{\tfrac{4}{9}[(A+C)-(B+D)]^2+(A-C)^2\}^{1/2}\,.\end{aligned}\tag{22}$$

The remaining off-diagonal elements are

$$\begin{aligned}&\langle g+|\mathcal{H}_{\mathrm{ex}}|e-\rangle=-(\sqrt{\tfrac{3}{2}})F\,,\\&\langle g+|\mathcal{H}_{\mathrm{ex}}|f-\rangle=(2E-F)/\sqrt{6}\,.\end{aligned}\tag{23}$$

The $S=1$, $M_s=1$ functions are

$$\begin{aligned}|h+\rangle&=E^a_{\theta,1/2}E^b_{\theta,1/2}\,,\\|i+\rangle&=E^a_{\epsilon,1/2}E^b_{\epsilon,1/2}\,,\\|j+\rangle&=\frac{1}{\sqrt{2}}(E^a_{\epsilon,1/2}E^b_{\theta,1/2}+E^a_{\theta,1/2}E^b_{\epsilon,1/2})\,,\end{aligned}$$

$$|j-\rangle=\frac{1}{\sqrt{2}}(E^a_{\epsilon,1/2}E^b_{\theta,1/2}-E^a_{\theta,1/2}E^b_{\epsilon,1/2}).\tag{24}$$

The diagonal matrix elements of $\mathcal{H}_{\mathrm{ex}}$ are

$$\begin{aligned}&\langle h+|\mathcal{H}_{\mathrm{ex}}|h+\rangle=2R-\tfrac{1}{4}B\,,\\&\langle i+|\mathcal{H}_{\mathrm{ex}}|i+\rangle=2R+\tfrac{1}{36}[-8(A+C)-(B-8D)]\,,\\&\langle j+|\mathcal{H}_{\mathrm{ex}}|j+\rangle=2R+\tfrac{1}{12}[-2(A-C)+(B-4D)]\,,\\&\langle j+|\mathcal{H}_{\mathrm{ex}}|j-\rangle=2R+\tfrac{1}{12}[2(A-C)+(B-4D)]\,.\end{aligned}\tag{25}$$

The off-diagonal matrix element between the $|h+\rangle$ and $|i+\rangle$ states is

$$\langle i+|\mathcal{H}_{\mathrm{ex}}|h+\rangle=-(A-C)/6\tag{26}$$

and the energies of the $|h+\rangle$ and $|i+\rangle$ states are

$$\begin{aligned}E=2R&-\tfrac{1}{36}[4(A+C)+(5B-4D)]\\&\pm\tfrac{1}{6}\{\tfrac{4}{9}[(A+C)-(B+D)]^2+(A-C)^2\}^{1/2}\,.\end{aligned}\tag{27}$$

The remaining off-diagonal terms are

$$\begin{aligned}&\langle j-|\mathcal{H}_{\mathrm{ex}}|h+\rangle=F/\sqrt{6}\\&\langle j-|\mathcal{H}_{\mathrm{ex}}|i+\rangle=-(2E-F)/3\sqrt{6}\,.\end{aligned}\tag{28}$$

Thus the effects of the exchange interaction on the $S=1$ levels are one-third as large as for the $S=0$ levels and have the opposite signs leaving the center of gravity unchanged.

Up to this point the effect of the crystal field on the ${}^2E$ state has not been taken into account. From the single-ion spectrum, the combined effects of the trigonal field and spin-orbit coupling yield a splitting of 5.4 cm^{-1} and this is sufficiently small to be neglected. A possibly much larger crystal-field splitting is the low symmetry distortion resulting from the close proximity of the nn Cr^{3+} ion. From the pair symmetry, this effect is expected to be strongest along the pair axis, and will change the ${}^2E-{}^4A_2$ separation as well as the ${}^2E_\theta-{}^2E_\epsilon$ splitting. We show in Sec. VI that for the single excited pair states these effects are also considerably smaller than the exchange splittings.

B. Transition Probabilities and Polarization

The experimental evidence of Sec. II suggests that the strongest pair transitions obtain their strength from the exchange-induced dipole moment.[31] With this mechanism the optical electric field, via its effect on the exchange interaction, induces a polarization

$$\vec{\mathrm{P}}=-\frac{\partial\mathcal{H}_{\mathrm{ex}}}{\partial\vec{\mathrm{E}}}\,.\tag{29}$$

This can be rewritten in terms of the single electron-spin operators

$$\vec{P} = \sum \vec{P}_{ij}\, \vec{s}_i \cdot \vec{s}_j , \tag{30}$$

where the $\vec{P}_{ij}$ are expressed in terms of the electric field dependence of the exchange parameters

$$\vec{P}_{ij} = \frac{\partial J_{ij}}{\partial \vec{E}} . \tag{31}$$

Explicit quantum-mechanical expressions for $\vec{P}_{ij}$ have been given.[31] However, the numerical evaluation of these expressions is at least as difficult as the first-principles calculation of the exchange parameters. Hence as was done for the J_{ij}, we treat the dipole moments as empirical parameters.

The number of independent $\vec{P}_{ij}$ is determined by the symmetry of the pair. For this purpose it is convenient to define the vector part of $\vec{P}_{ij}$ in the XYZ coordinate frame of Fig. 2 but retain the x, y, z frame for the i, j indices. In the ideal perovskite structure the presence of a center of inversion at the oxygen site gives $\vec{P}_{ij} = -\vec{P}_{ji}$. Together with the remaining symmetry operations, this leads to a vanishing of the dipole moment if the same symmetry final states are involved. As is indicated in Sec. VIC, the dipole moment does *not* vanish if the final state of the pair consists of ions in different states, for example, the $^4A_2$ and ^2E states, or the doubly excited state with one ion in the $^2E_\theta$ state and the other in the $^2E_\epsilon$ state. With the lower symmetry of the actual pair the C_{2X} operation leaves the X component invariant and we obtain six independent dipole moments,

$$\begin{gathered} P_{11}^X = P_{22}^X,\ P_{33}^X,\ P_{12}^X, \\ P_{21}^X,\ P_{13}^X = P_{32}^X,\ P_{31}^X = P_{23}^X . \end{gathered} \tag{32}$$

The Z component changes sign under C_{2X}, hence

$$\begin{gathered} P_{11}^Z = -P_{22}^Z,\quad P_{33}^Z = 0,\quad P_{12}^Z = P_{21}^Z = 0, \\ P_{13}^Z = -P_{32}^Z,\quad P_{31}^Z = -P_{23}^Z, \end{gathered} \tag{33}$$

and similar expressions obtain for the Y component.

The matrix elements are calculated in the same manner as the exchange splittings. The dipole moments of each of the $\Delta S = 0$, $\Delta M_s = 0$ transitions from the ground state to the singly excited states are the following:

For $S = 1$,

$$\vec{P} = \begin{array}{cccc} \langle AA+|\vec{P}|a+\rangle & \langle AA+|\vec{P}|a-\rangle & \langle AA+|\vec{P}|b+\rangle & \langle AA+|\vec{P}|b-\rangle \\ \end{array}$$

$$\vec{P} = \left(\begin{array}{cccc} 0 & -(\sqrt{5}/3\sqrt{6})[(P_{12}^X - P_{21}^X) + (P_{13}^X - P_{31}^X)] & \begin{array}{c} (\sqrt{5}/9\sqrt{2})[2(-P_{11}^X + P_{33}^X) \\ -(P_{12}^X + P_{21}^X)] + (P_{31}^X + P_{13}^X) \end{array} & 0 \\ -(\sqrt{5}/3\sqrt{6})(2P_{11}^Y + P_{13}^Y + P_{31}^Y) & 0 & 0 & (\sqrt{5}/3\sqrt{2})(P_{31}^Y - P_{13}^Y) \\ -(\sqrt{5}/3\sqrt{6})(2P_{11}^Z + P_{13}^Z + P_{31}^Z) & 0 & 0 & (\sqrt{5}/3\sqrt{2})(P_{31}^Z - P_{13}^Z) \end{array} \right) ; \tag{34}$$

and for $S = 2$,

$$\vec{P} = \left(\begin{array}{cccc} \langle AA-|\vec{P}|c+\rangle & \langle AA-|\vec{P}|c-\rangle & \langle AA-|\vec{P}|d+\rangle & \langle AA-|\vec{P}|d-\rangle \\ (1/\sqrt{6})[(P_{12}^X - P_{21}^X) + (P_{13}^X - P_{31}^X)] & 0 & 0 & \begin{array}{c} (1/3\sqrt{2})[2(P_{11}^X - P_{33}^X) \\ +(P_{12}^X + P_{21}^X)] - (P_{13}^X + P_{31}^X) \end{array} \\ 0 & (1/\sqrt{6})(2P_{11}^Y + P_{13}^Y + P_{31}^Y) & (1/\sqrt{2})(P_{13}^Y - P_{31}^Y) & 0 \\ 0 & (1/\sqrt{6})(2P_{11}^Z + P_{13}^Z + P_{31}^Z) & (1/\sqrt{2})(P_{13}^Z - P_{31}^Z) & 0 \end{array} \right) . \tag{35}$$

Comparing the transitions having the same combination of $\vec{P}_{ij}$ parameters shows that the ratio of the $S = 1$ to $S = 2$ dipole moments is $-\frac{1}{3}\sqrt{5}$.

The dipole moments to each of the doubly excited states are, for $S = 0$,

$$\vec{P} = \left(\begin{array}{cccc} \langle AA-|\vec{P}|e-\rangle & \langle AA-|\vec{P}|f-\rangle & \langle AA-|\vec{P}|g+\rangle & \langle AA-|\vec{P}|g-\rangle \\ (1/2\sqrt{2})[2P_{11}^X - (P_{12}^X + P_{21}^X)] & \begin{array}{c} (1/6\sqrt{2})[2P_{11}^X + P_{12}^X + P_{21}^X \\ +4(P_{33}^X - P_{13}^X - P_{31}^X)] \end{array} & (1/2\sqrt{3})[P_{21}^X - P_{12}^X + 2(P_{31}^X - P_{13}^X)] & 0 \\ 0 & 0 & 0 & (1/\sqrt{3})(P_{11}^Y - P_{13}^Y - P_{31}^Y) \\ 0 & 0 & 0 & (1/\sqrt{3})(P_{11}^Z - P_{13}^Z - P_{31}^Z) \end{array} \right) , \tag{36}$$

and for $S=1$,

$$\vec{\mathrm{P}}=\begin{array}{cccc} \langle AA+|\vec{\mathrm{P}}|h+\rangle & \langle AA+|\vec{\mathrm{P}}|i+\rangle & \langle AA+|\vec{\mathrm{P}}|j+\rangle & \langle AA+|\vec{\mathrm{P}}|j-\rangle \\ \left(\begin{array}{c} (\sqrt{10}/12)[2P^X_{11}-(P^X_{12}+P^X_{21})] \\ \\ 0 \\ 0 \end{array}\right. & \begin{array}{c} (\sqrt{5}/18\sqrt{2})[2P^X_{11}+P^X_{12}+P^X_{21} \\ \quad +4(P^X_{33}-P^X_{31}-P^X_{13})] \\ 0 \\ 0 \end{array} & \begin{array}{c} 0 \\ \\ (\sqrt{5}/3\sqrt{3})(P^Y_{11}-P^Y_{13}-P^Y_{31}) \\ (\sqrt{5}/3\sqrt{3})(P^Z_{11}-P^Z_{13}-P^Z_{31}) \end{array} & \left.\begin{array}{c} (\sqrt{5}/6\sqrt{3})[P^X_{21}-P^X_{12}+2(P^X_{31}-P^X_{13})] \\ \\ 0 \\ 0 \end{array}\right) \end{array}. \tag{37}$$

Both the single and double excitations thus have well-defined polarization characteristics. The relative magnitudes of the $\vec{\mathrm{P}}_{ij}$ components are more difficult to establish than was the case for the J_{ij}. However, as a lowest-order approximation let us assume the relative polarizabilities of the J_{ij} to be equal. Hence, $\vec{\mathrm{P}}_{ij}\propto J_{ij}$, and the dominant contribution is expected to come from $\vec{\mathrm{P}}_{11}$, with the $\vec{\mathrm{P}}_{12}$ term much smaller, the remaining components being negligible. The strongest single excitation transitions are thus to the $|b+\rangle$ and $|d-\rangle$ states in σ polarization and to $|a+\rangle$ and $|c-\rangle$ in both σ and π polarization. For the uv, the transitions to both of the admixed $|e-\rangle$, $|f-\rangle$ states as well as the pair of $|h+\rangle$, $|i+\rangle$ states will be strictly σ polarized, while the transitions to the $|g-\rangle$ and $|j+\rangle$ states appear strongly in σ and π polarization. The transitions to the remaining levels are expected to be relatively weak.

The dipole moment $\vec{\mathrm{P}}$ commutes with the total spin operator $\vec{\mathrm{S}}$, and for a given $\vec{\mathrm{S}}$ each of the M_s levels have equal dipole moments. Hence, the absorption coefficient is proportional to the square of the dipole moment, Eqs. (34)–(37) times the population of the initial level.

VI. COMPARISON WITH EXPERIMENT

A. Singly Excited States

The theoretical expressions for the intensities and polarizations developed above are compared in this section with the observed transitions. For the singly excited pair levels the 13 366. 9 and 13 701 cm^{-1} appear in both σ and π polarizations and are identified with the $|c-\rangle$ and $|a+\rangle$ states. Similarly the σ- and α-polarized lines at 13 562. 4 and 13 794 cm^{-1} are associated with the $|b+\rangle$ and $|d-\rangle$ states. A further check of the theory is obtained by comparing the relative intensities of Table III with the values calculated from Eqs. (34) and (35). At 137 °K the ratio of the $S=1$ to $S=2$ intensity is computed to be

$$(\sqrt{5}/3)^2(0.46/0.18)=1.42,$$

where the first factor is the ratio of the square of the dipole moments and the second factor is the ratio of the $S=1$ to $S=2$ populations (Fig. 7). From Table III we find the measured ratios for the $|a+\rangle$ and $|c-\rangle$ states to be 1.29 and 1.2 for the σ and π components, respectively. Similar results are obtained using the 77 °K data. Considering the accuracy of the measurements the agreement is quite good. For the σ-polarized lines the ratio is found to be 5 which is significantly larger than the calculated value. The origin of this difference is not completely understood. However, it appears that the broad 13 957-cm^{-1} line has, by an unknown mechanism, borrowed most of the σ intensity from the 13 794-cm^{-1} line. By adding the intensities of these two lines we obtain an $S=1$ to total $S=2$ intensity ratio of 1.31 which is close to the ratio obtained for the other lines. The energy levels of the single excited pair states are shown in Fig. 12(a). The appropriate ground-state splitting of

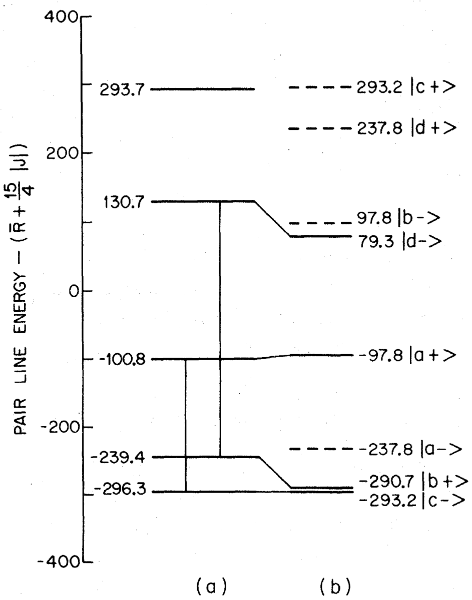

FIG. 12. Effect of exchange on the singly excited pair states. (a) Measured splittings of the $S=1$ and 2 levels. (b) Splittings calculated using $A=-531.1$ cm^{-1} and $C=55.4$ cm^{-1}.

each transition was added to the measured energy and 13 873.3 cm^{-1} was subtracted. The latter consist of the average single-ion ^2E_g-$^4A_{2g}$ separation $\bar{R}$, and the $\frac{15}{4}|J|$ depression of the $S=0$ ground-state level.

In order to evaluate the J_{ij} parameters we use the approximations suggested by Anderson, and retain only the A and C terms.[32] As indicated in Sec. V the main contribution of the crystal field is expected to be an axial distortion along the pair z axis, which contributes to the splitting of the single-ion $^2E_\epsilon$ and $^2E_\theta$ levels. By evaluating the parameters using the energy differences within the single-ion $^2E_\epsilon$ and $^2E_\theta$ levels of the pair, this crystal-field effect is minimized. For the pair of energy separations shown in Fig. 12(a) by the vertical lines we obtain $A=-531.1$ cm^{-1} and $C=55.4$ cm^{-1}. Substituting these values back into Eqs. (12) and (15) results in the calculated level splittings shown in Fig. 12(b). The difference in the separation from the center of gravity for the calculated and experimental energies of the $|a+\rangle$ and $|c-\rangle$ states is 3 cm^{-1}; whereas for the $|d-\rangle$ and $|b+\rangle$ states this difference is 51.3 cm^{-1}. In addition, we see that the calculated energy of the $|c+\rangle$ state is quite close to the measured highest-energy pair level. The small difference essentially justifies the neglecting of these terms in our calculation.

With these A and C values for the exchange parameters, the calculated ground state J^{ab} is -105.7 cm^{-1}. This is about 50% larger than the measured value. That the exchange parameters are larger in the excited state is due in part to the smaller energy denominator U in the expression for the kinetic exchange, Eq. (7). If we assume this to be the sole source of the exchange enhancement, we find that U for the ground-state kinetic exchange is about 5 eV, which is one-half the value suggested by Anderson.[32] Another contribution comes from the following mechanism: The theory has made use only of the spherical symmetry of the wave functions. A small radial dilatation of the excited-state wave function caused by an about 5% admixture of the t^2e orbitals from $^4T_{2g}$ will tend to increase the overlap integrals and hence yield a larger exchange.

B. Doubly Excited States

The low-temperature uv lines (Fig. 10) at 26 701 and 27 758 cm^{-1} appearing in σ and α polarization are identified as the transitions to the coupled $|e-\rangle$ and $|f-\rangle$ states. Assuming the $\vec{P}_{11}$ dipole moment is dominant, the transition to $|g-\rangle$ has the same polarization as the transitions to $|a+\rangle$ and $|c-\rangle$, and will thus appear most strongly in π polarization. The identification of the 27 343-cm^{-1} absorption as this transition is verified by its π-to-σ ratio of 2.1 which compares with a similar ratio 2.2 ± 0.1 for the $|a+\rangle$ and $|c-\rangle$ transitions (Table III). The theory predicts the remaining transition to $|g+\rangle$ to be quite weak and we have not been able to separate this transition from the vibronics.

The $S=1$ transition at 27 063 cm^{-1} and the tentatively identified transition at 27 402 cm^{-1} are identified with the transitions to the mixed $|h+\rangle$ and $|i+\rangle$ states, and the 26 701-cm^{-1} absorption is tentatively identified with the transition to $|j+\rangle$. The weak transition to $|j-\rangle$ has not been identified.

The experimentally determined level positions are shown in Fig. 13(a). In order to compare with the theory, we have subtracted $2\bar{R}+\frac{15}{4}|J| = 27\,499$ cm^{-1} from the measurements. The centers of gravity of the σ and mainly π absorption levels are shown between the $S=0$ and 1 diagrams. Figure 13(b) shows the splitting patterns calculated using the previously determined $A+C$ parameters. The splittings of the $S=0$ $|ef-\rangle$ and the $S=1$ $|hi+\rangle$ which appear in σ and α polarizations have approximately the predicted 3:1 ratio. However,

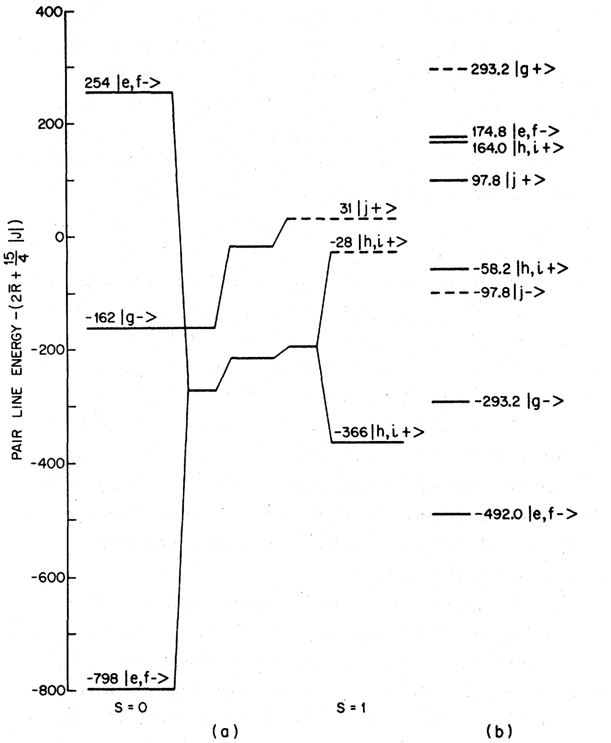

FIG. 13. Effect of exchange on the doubly excited pair states. (a) Measured splittings of the $S=0$ and 1 levels. The dashed lines indicate the positions of the electronic level which are partially obscured by the vibronics. The centers of gravity are shown between the curves. (b) Splittings calculated using $A=-531.1$ cm^{-1} and $C=55.4$ cm^{-1}.

although these splittings are substantially larger than the calculated values, the shift, given by $\frac{1}{3}(A+C)$ for $S=0$ [Eq. (22)], is substantially smaller than calculated, and the center of gravity of this set of levels is 216 cm^{-1} below the calculated zero. These effects are apparently related to the phonon coupling. The energy separation between the $S=0$ and 1 levels which appear mainly in π polarization has about one-half the calculated value. In this case the center of gravity is only 17 cm^{-1} below the calculated zero. In both cases the signs of the exchange shifts agree with theory. The agreement between the experimental and calculated splittings shown in Fig. 13 is rather disappointing in this case.

C. Vibronic Effects

The theoretical intensity ratios of the σ-polarized uv transitions are not observed. For example, the ratio of the absorption coefficients of the upper 27 063-cm^{-1} $S=1$ $|hi+\rangle$ transition to the lower 27 758-cm^{-1} $S=0$ $|ef-\rangle$ transition is calculated to be 0.47 at 82 °K, whereas the measured ratio is about 15. In fact most of the dipole strength has been transferred to the lowest energy levels. In addition, we find that only these transitions are strongly coupled to the lattice vibrations. These anomalous effects are due to the special nature of the final states, in which *both* ions of the pair are in either the $^2E_\theta$ or the $^2E_\epsilon$ single-ion states. We indicated in Sec. V that the dipole moments vanished in the cubic perovskite phase, and at low temperatures exist only by virtue of the rhombohedral distortion. This assumes the t_{2g} orbitals are identical in the $^4A_2$, $^2E_\theta$, and $^2E_\epsilon$ states. However, we have found that the exchange is considerably larger in the singly excited pair state, thus implying that a given t_{2g} orbital is not precisely the same in these three states. In this case, the pair absorption does not vanish in the perovskite phase if the final states are different. The polarization of the low-temperature absorption is essentially unchanged by this modification. This argument does not apply when the final states of the pair are the same, and these dipole moments vanish in the cubic phase.

We want to emphasize the importance of the rhombohedral distortion on the vibronic spectrum. In the low-temperature Raman spectrum, Scott has observed the "soft" E_g mode at 40 cm^{-1} and the A_{1g} mode at 147 cm^{-1} of the LaAlO_3 host which are associated with the cubic to rhombohedral phase transition.[33] At 300 °K additional Raman-active phonon modes are observed at 470 and 487 cm^{-1}. Weak but well-defined vibronics of the single-ion R-line spectrum are observed at 105, 146, 337, and 403 cm^{-1} from the R lines (Fig. 3), and also quite strong broader vibronics at 654 and 767 cm^{-1}.

For the vibronics of the 26 706-cm^{-1} transition the following phonon separations (in parentheses) are observed: 26 582 (146) appears in σ polarization, and the following are unpolarized vibronics: 26 997 (2×145.5), 27 108 (402), 27 285 (4×145), 27 457–27 480 (751–779), 27 580 (6×145.6), and 28 260 (2×777) cm^{-1}. The separations of the absorption at 26 761–26 773 (55–67) and 27 904 (208) cm^{-1} from the 26 706-cm^{-1} line do not appear in either the infrared pair or Raman spectra.

The phonon coupling of the $S=1$ 27 063-cm^{-1} transition is again strong with a σ-polarized sideband at 27 210 (147), and well-defined unpolarized sidebands at 27 647 (4×146), 27 723 (660), and 27 810–27 834 (747–771).

These σ-polarized lines thus couple most strongly to the A_{1g} mode at 147 cm^{-1} as well as to the strong unidentified phonon at ~770 cm^{-1}. The upper σ-polarized transitions do not show such a strong coupling. Weak vibronics of the 27 343-cm^{-1} transition, which have predominantly π polarization, are observed at 27 406 (63) cm^{-1} and 27 556 (213) cm^{-1}.

VII. SUMMARY AND CONCLUSIONS

In this paper we compare the results of a detailed experimental investigation of the nearest-neighbor spectrum of Cr^{3+} pairs in LaAlO_3 with the theory based on the single-electron–single-electron exchange Hamiltonian, Eq. (1), and the spin-induced electric dipole moment, Eq. (30). Due to its crystallographic structure this host leads to a simpler pair spectrum than is observed in ruby, and the spectrum is consequently more easily amenable to analysis. From the polarization and Zeeman effect we have confirmed that the pair transitions gain their intensity from the exchange-induced electric dipole moment mechanism. The analysis of the infrared pair spectrum involving one ion in the ^2E state and the second ion in the $^4A_2$ state resulted in a new value of the ground-state exchange and several of the excited-state splittings. The latter levels were used to determine the single-electron–single-electron exchange parameters J_{11} and $(J_{12}+J_{21})/2$. Reasonably good agreement between theory and experiment is found.

The pair absorption resulting from the promotion of both ions to the ^2E states was also observed. In this case the analysis and comparison with theory is complicated by the presence of a strong vibronic spectrum which results from the soft mode of the host. Only qualitative agreement with the theory was found in this case.

These pair transitions involve a spin flip within the half-filled $(t_{2g})^3$ shell. The transitions to the $^2T_{1g}$ and $^2T_{2g}$ states have also been examined. The strongest transition of the former is at ~14 362 cm^{-1}, and the latter consists of three absorption lines at 21 163.4 ($2\bar{A}$), 21 204.4 ($\bar{E}$), and 21 278.1 ($\bar{E}$) cm^{-1}. The strong-field wave functions of these states are made up of combinations of t_{2g} orbitals with two electrons in the same orbital state and with opposite spins and the third electron in a different orbital state.[34] The transitions to the ^2T states thus involve an orbital change as well as a spin flip. The theory described in Sec. V does not include this case. Such pair transitions become allowed through wave-function admixture, and are expected to be substantially weaker than the spin-flip transitions. Experimentally they are too weak to be identified.

The attempt to compare theory with experiment has been at least partially successful. As pointed out in Sec. VI, however, complete agreement has not been obtained. The discrepancies are of considerable interest, and require further study. The results clearly illustrate the importance of studying pairs in a simple well-defined symmetry. The perovskite structure, and its distorted modifications, provide ideal hosts for these investigations. The pair spectra in these hosts are expected to differ only in detail from the results presented here. For example, a very similar singly and doubly excited state spectrum of Cr^{3+} pairs has been observed in the orthorhombic host $YAlO_3$.[35]

ACKNOWLEDGMENTS

I am grateful to M. H. L. Pryce for a report of his unpublished work on the exchange interactions of Cr^{3+} pairs in ruby. I am also indebted to M. D. Sturge, R. C. Miller, S. E. Stokowski, and E. Cohen for helpful discussions during the course of this work, to M. Marezio and P. Dernier for use of their x-ray data prior to publication, to C. D. Brandle, Jr., for growing the several crystals as well as for discussions on detwinning and annealing, to R. T. Lynch for annealing the crystals, and to A. A. Ballman for the use of his detwinning apparatus.

---

[1] For a compilation of recent experimental work and references see P. Kisliuk, N. C. Chang, P. L. Scott, and M. H. L. Pryce, Phys. Rev. 184, 367 (1969).

[2] M. J. Berggren, G. F. Imbusch, and P. L. Scott, Phys. Rev. 188, 675 (1969).

[3] P. Kisliuk and W. F. Krupke, Appl. Phys. Letters 3, 215 (1963).

[4] J. H. Van Vleck, Rev. Mat. Fis. Teor. Univ. Nac. Tucuman 14, 189 (1962).

[5] A. M. Clogston (unpublished).

[6] A. E. Nikiforov and V. I. Cherpanov, Phys. Status Solidi 14, 391 (1966).

[7] N. L. Huang, Phys. Rev. B 1, 945 (1970).

[8] M. H. L. Pryce (unpublished).

[9] K. W. Blazey and G. Burns, Phys. Letters 15, 117 (1965).

[10] A. M. Tkachuk and Z. N. Zonn, Opt. i Spektroskopiya 26, 587 (1969) [Opt. Spectry. (USSR) 26, 322 (1969)]; Z. N. Zonn, V. A. Ioffe, and P. P. Feofilov, *ibid.* 19, 973 (1965) [19, 541 (1965)].

[11] Cr^{3+} pair emission was also observed by F. Forrat, R. Jansen, and P. Trévoux, Compt. Rend. 256, 1271 (1963); L. Couture, F. Brunetiere, F. Forrat, and P. Trévoux, *ibid.* 256, 3046 (1963).

[12] J. P. van der Ziel, Phys. Rev. Letters 26, 766 (1971).

[13] S. Geller and V. B. Bala, Acta Cryst. 9, 1019 (1956).

[14] S. Geller, Acta Cryst. 10, 248 (1957).

[15] M. Marezio, J. P. Remeika, and P. D. Dernier (unpublished).

[16] *International Tables for X-Ray Crystallography*, edited by N. F. M. Henry and K. Lonsdale (Kynoch Press, Birmingham, England, 1952), Vol. 1, p. 274.

[17] K. A. Müller, W. Berlinger, and F. Waldner, Phys. Rev. Letters 21, 814 (1968); K. A. Müller and W. Berlinger, *ibid.* 26, 13 (1971).

[18] J. D. Axe, G. Shirane, and K. A. Müller, Phys. Rev. 183, 820 (1969).

[19] H. Fay and C. D. Brandle, J. Appl. Phys. 38, 3405 (1967).

[20] H. Fay and C. D. Brandle, in *Crystal Growth*, edited by E. S. Peiser (Pergamon, Oxford, England, 1967), p. 51.

[21] J. S. Smart, in *Magnetism*, edited by G. Rado and H. Suhl (Academic, New York, 1963), Vol. III, p. 63.

[22] J. P. van der Ziel and L. G. Van Uitert, Phys. Rev. 179, 343 (1969).

[23] G. H. Jonker, Physica 22, 707 (1956).

[24] W. C. Koehler and E. O. Wollan, J. Phys. Chem. Solids 2, 100 (1957).

[25] G. S. Rushbrooke and P. J. Wood, Mol. Phys. 6, 409 (1963).

[26] L. F. Mollenauer and A. L. Schawlow, Phys. Rev. 168, 309 (1968).

[27] A. A. Kaplyanskii and A. K. Przhevuskii, Dokl. Akad. Nauk SSSR 142, 313 (1962) [Sov. Phys. Doklady 7, 37 (1962)].

[28] A. A. Kaplyanskii and A. K. Przhevuskii, Fiz. Tverd. Tela 9, 190 (1967) [Sov. Phys. Solid State 9, 190 (1967)].

[29] M. D. Sturge, Phys. Rev. 140, A880 (1965). This apparatus follows the design described by A. L. Schawlow, A. H. Piksis, and S. Sugano, Phys. Rev. 122, 1469 (1961).

[30] D. Kiro, W. Low, and Z. Zusman, *Paramagnetic Resonance* (Academic, New York, 1963), Vol. 1, p. 44.

[31] Y. Tanabe, T. Moriya, and S. Sugano, Phys. Rev. Letters 15, 1023 (1965); K. I. Gondaira and Y. Tanabe, J. Phys. Soc. Japan 21, 1527 (1966); Y. Tanabe and K. I. Gondaira, *ibid.* 22, 573 (1967); see also R. Loudon, Advan. Phys. 17, 243 (1968).

[32] P. W. Anderson, in *Solid State Physics*, edited by F. Seitz and D. Turnbull (Academic, New York, 1963), Vol. 14, p. 99.

[33] J. F. Scott, Phys. Rev. 183, 823 (1969). The energies of the E_g and A_{1g} phonons were accidently reversed in Ref. 12.

[34] J. S. Griffith, *Theory of Transition Metal Ions* (Cambridge U.P., Cambridge, England, 1961), p. 406.

[35] J. P. van der Ziel (unpublished).